JOURNAL OF MATERIALS SCIENCE **38** (2003) 3269–3278

Effects of interface properties on densification in a grain compact during sintering

H. CAMACHO, M. E. FUENTES, L. FUENTES
Advanced Materials Research Center (CIMAV), Ceramics Division, Chihuahua, Chihuahua, 31109, Mexico
E-mail: hcamacho@mailaps.org

A theoretical approach to describe the relationship between the interface properties and densification for sintering materials is presented. This approach is developed by assuming simplified grain boundary geometry, where scaling is imposed. In general, the results are in good agreement with theoretical calculations from other studies, as well as with available experimental data. The model predicts a higher densification rate in particle agglomerates, if grain growth is inhibited. Hence, qualitative predictions lead to a plausible explanation, for instance, for the effect of niobium doping on PZT ceramics experimentally reported in the literature. The bulk and shear viscosities, as well as the sintering stress are reported.

1. Introduction

Ceramic processing theories, modeling and simulations are powerful tools for rationally designing sintered ceramic bodies with specific properties. Further progress in this area requires integrating together the theoretical descriptions that have been developed at different length scales (L), i.e., atomistic ($L \sim 10^{-9}$ m), mesoscopic ($L \sim 10^{-6}$ m) and macroscopic ($L \sim 10^{-3}$ m).

During the last few decades, there have been significant developments in sintering theory. The assumption of viscous behavior during sintering has proven to be useful for describing this phenomenon in amorphous materials. Frenkel [1] and Mackenzie and Shuttlewoth [2] made pioneering contributions in this field.

The application of continuum theories to describe macroscopic-level phenomena has developed rapidly in recent years. Bordia and Scherer [3] have reviewed many of these theories, and have studied the viscous behavior during sintering.

Macroscopic models accept any macroscopic properties, regardless of their cause. The viscous properties may also be calculated using mesoscopic models. Unlike continuum theories, the mesoscopic models are more focused on the sintering phenomenon itself. Scherer Cell Model [4], as well as the models developed by Martínez-Herrera and Derby [5] and Van de Vorst [6], using the Navier-Stokes fluid equation, are examples in this respect.

For polycrystals, intermediate and final stages of sintering have been defined by Coble [7]. Based on these definitions, and applying Fick's Laws of Difussion at the mesoscopic level, Riedel and co-workers developed a diffusional model that can be used to describe the macroscopic viscous behavior of polycrystals [8–11]. The use of Fick's laws to describe mass transport during sintering, was also considered by Cock *et al*. [12, 13] and Zhang *et al*. [14] In general, different sintering mechanisms may be activated during the sintering of polycrystals [15], and many of them can be well modeled using Fick's laws. Viscous sintering in packed particles has also been studied by Jagota and coworkers [16–18]. However, sintering theory for polycrystalline agglomerates is far from being complete, and it requires further research and study.

Also, much of the recent theoretical work has focused on grain growth evolution, thus providing a better insight in this matter [19–23]. The models resulting from these studies describe the mesostructural evolution which, in fact, has a significant influence on the macroscopic sintering behavior.

In this paper, we consider a compact having an idealized simplified grain-boundary geometry, where scaling [19–21] is imposed. Hence, the final behavior results from the both conditions. Section 2 describes the model used in this study. The results are included in Section 3. Discussions, as well as the interpretation of some experimental results reported in literature, are presented in Section 4.

2. Starting hypothesis and governing relations

We use a somewhat simplified model able to simulate the most important characteristics of grain agglomerates at a mesoscopic level. The mesocell is defined by choosing a volume with constant mass. From this geometry, it is possible to determine the most common relations for describing the sintering process. Most of the properties are calculated following the Riedel methodology, so it must be pointed out that there is a remarkable difference between the corresponding

mesocells. The Riedel mesocell or the Wigner-Seitz cell is a tetrakaidekahedron related to one grain, as normal grain growth takes place the mesocell mass varies. For the present work, grain growth leads to decrease the related number of grains per mesocell.

2.1. Geometrical relations

We consider the mesocell shown in Fig. 1, where l and h are the lateral dimension and the thickness, respectively. Sintering takes place in two dimensions $l \times l$, h remains constant during all the process. The plane of the figure is parallel to the $l \times l$ plane. We study the relative density, ρ, from 0.65 to 1.0. The intermediate and final stages are represented by stage I ($\rho = 0.65$–0.9) with $n_p + n_p^I$ pores and stage II ($\rho = 0.9$–1.0) with n_p pores. Then, n_p^I pores collapse for $\rho_{pc} = 0.9$. Three kinds of grain boundaries are defined and we name them as C_1, C_2, and C_{12}. The number of pores n_p and n_p^I; grain contacts, $n(C_1)$, $n(C_2)$, and $n(C_{12})$; and grains, n_{lg}, n_{mg}, and n_{sg}, are given by the following recurrent relations

$$\begin{aligned} &n_p = 14n^2 \quad n(C_1) = n(C_2) = 4n^2 \quad n_{1g} = 2n^2 \\ &n_p^1 = 16n^2 \quad n(C_{12}) = 56n^2 \qquad\quad n_{mg} = 16n^2 \\ &\qquad\qquad\qquad\qquad\quad n_{sg} = 16n^2 \end{aligned} \tag{1}$$

where n is an intrinsic real index that describes the evolution of the system. Fig. 1 shows the $n = 1$ mesocell. For higher values of n, the qualitative picture of Fig. 1 is preserved. Sintering proceeds as n decreases. Linear dimensions fulfill the scaling principle. Then, linear dimensions of the grains are reduced by the factor $1/n$. The magnitudes $d(C_1)$, $d(C_2)$, and $d(C_{12})$ keep their relations according to the values of n and the grain boundary orientation remain unchangeble for all n values.

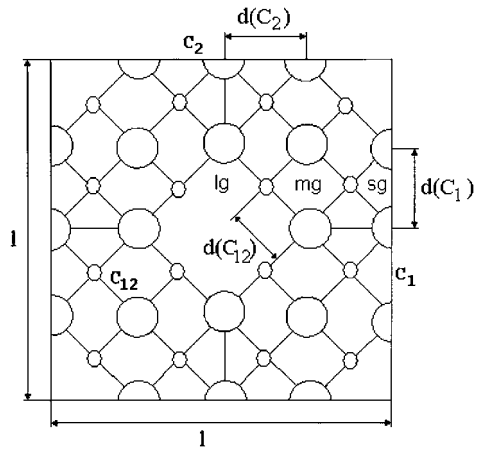

Figure 1 The $l \times l$ plane view of the mesocell for $n = 1$. The circles, which are cylinders in three dimensions, represent the cell pores and the areas not included in the spheres represent the cell grains. Straight lines are the grain boundaries, which are assumed to have curvatures in the calculation. Three kinds of grain boundaries C_1, C_2, and C_{12} are defined and three kind of grains *lg* (large size grain), *mg* (middle size grain), and *sg* (small size grain). The h thickness dimension remains constant during all the process. The smallest pores are those named as n_p^I pores in this work. The collapse of n_p^I pores defines the end of stage I. The rest of the pores are known as n_p pores and collapse for $\rho = 1.0$.

Pore reduction implies that the relation $r/d(C_{12})$ varies as sintering proceeds and scaling is violated is this sense. Resuming, all mentioned assumptions are simplified descriptions of experimentally reported behaviors. They are consistent with the Statistical Self Similarity hypothesis [19–21].

The relative density of the grain compact may be defined as:

$$\rho = \frac{V_s}{V} \tag{2}$$

where V and V_s correspond, respectively, to volume of the mesocell and volume of the solid part of it. ($V = V_s$ for $\rho = 1$) They are related as shown:

$$V = V_s + n_p \pi r_n^2 h + n_p^I \pi r_n^{I^2} h \tag{3}$$

where r_n and r_n^I are the pore radius of the n_p and n_p^I pores respectively related to the intrinsic parameter n. Note that, $r_n = r_n^I = 0$ implies that $\rho = 1$.

The following equations express the relation among l, l_s, r_n, and r_n^I, where l and l_s are the cell lateral dimensions for $V = l^2 h$ and $V_s = l_s^2 h$ respectively:

$$\begin{aligned} hl^2 &= hl_s^2 + 14n^2 \pi r_n^2 h + 16n^2 \pi r_n^{I^2} h \\ &= hl_s^2 + 14\pi r_{n=1}^2 h + 16\pi r_{n=1}^{I^2} h \end{aligned} \tag{4}$$

The constant parameter l_s represents the cell lateral dimension for $\rho = 1$. Besides,

$$r_n = \frac{r}{n} \qquad r_n^I = \frac{r^I}{n} \tag{5}$$

and we take $r = r_{n=1}$ and $r^I = r_{n=1}^I$.

The system evolution rate (see Fig. 1) is defined as:

$$v_{se} = -\frac{l_s}{n_0} \frac{dn}{dt} \tag{6}$$

and the pore decrease velocity as:

$$v_{pd} = -\frac{dr}{dt}. \tag{7}$$

Now, n and r can be written from the above definitions as:

$$\begin{aligned} n(t) &= n_0 \left(1 - \frac{1}{l_s} \int_0^t v_{se}(t')\, dt' \right) \\ r(t) &= r_0 - \int_0^t v_{pd}(t')\, dt' \end{aligned} \tag{8}$$

Hence, the relative density takes the following form:

$$\rho = \frac{1}{1 + 14\pi \left(\alpha_0 - \frac{1}{l_s} I_{pd} \right)^2 + 16\pi \left(\alpha_0^I - \frac{1}{l_s} I_{pd}^I \right)^2} \tag{9}$$

where $I_{pd} = \int_0^t v_{pd}(t')\, dt'$, $\alpha_0 = r_0/l_s$, $I_{pd}^I = \int_0^t v_{pd}^I(t')\, dt'$, and $\alpha_0^I = r_0^I/l_s$. The parameters α_0 and α_0^I may be

calculated from

$$\begin{aligned}\rho_0 &= 0.65 = 1\Big/\left(1 + 14\pi\alpha_0 + 16\pi\alpha_0^{\mathrm{I}}\right)\\ \rho_{\mathrm{pc}} &= 0.9 = 1/(1 + 14\pi\alpha_9)\end{aligned} \tag{10}$$

where $\rho_0 = 0.65$ and $\rho_{\mathrm{pc}} = 0.9$ are taken as the green density, and the $n_{\mathrm{p}}^{\mathrm{I}}$ pore collapse density. The relation among α_0, α_0^{I}, and α_9 will be stated later. Densification rate is straightforward from

$$\varepsilon_\rho = \frac{\mathrm{d}\rho}{\mathrm{d}t} \tag{11}$$

The cross sectional areas of the idealized grains are given by:

$$\begin{aligned}A_{1\mathrm{g}} &= (2d(C_{12}))^2 - 4\left(\frac{1}{4}\pi r_{\mathrm{n}}^2\right) - 4\left(\frac{1}{2}\pi r_{\mathrm{n}}^{\mathrm{I}^2}\right) = \pi r_{1\mathrm{g}}^2\\ A_{\mathrm{mg}} &= d^2(C_{12}) - 2\left(\frac{1}{4}\pi r_{\mathrm{n}}^2\right) - 2\left(\frac{1}{4}\pi r_{\mathrm{n}}^{\mathrm{I}^2}\right) = \pi r_{\mathrm{mg}}^2\\ A_{\mathrm{sg}} &= \frac{1}{2}d^2(C_{12}) - 2\left(\frac{1}{8}\pi r_{\mathrm{n}}^2\right) - \left(\frac{1}{4}\pi r_{\mathrm{n}}^{\mathrm{I}^2}\right) = \pi r_{\mathrm{sg}}^2\end{aligned} \tag{12}$$

It is important to note that an effective grain radius was defined in the above equation, as if the idealized grains were spherical. Under this assumption, the average grain size can be calculated using the following equation.

$$\langle r_{\mathrm{gs}}\rangle = \frac{1}{n_{1\mathrm{g}} + n_{\mathrm{mg}} + n_{\mathrm{sg}}}(n_{1\mathrm{g}}r_{1\mathrm{g}} + n_{\mathrm{mg}}r_{\mathrm{mg}} + n_{\mathrm{sg}}r_{\mathrm{sg}}) \tag{13}$$

2.2. Scaling principle

Grain boundary velocities may be expressed as (Appendix 1):

$$\begin{aligned}v_{\mathrm{gb1}} = v_{\mathrm{gb2}} &= \frac{\mathrm{d}u_1}{\mathrm{d}t} = \frac{\mathrm{d}u_2}{\mathrm{d}t} \approx \frac{1}{2n}\frac{l}{l_{\mathrm{s}}}v_{\mathrm{se}}\\ v_{\mathrm{gb12}} &= \frac{\mathrm{d}u_{12}}{\mathrm{d}t} \approx \frac{\sqrt{2}}{8n}\frac{l}{l_{\mathrm{s}}}v_{\mathrm{se}}\end{aligned} \tag{14}$$

Assuming a steady-state condition for grain boundary migration [22], then

$$v_{\mathrm{gb}} = Mp \tag{15}$$

where p is the driving force or pressure, and M_{gb} is the mobility of the grain boundary, i.e., the velocity per unit driving force. Considering $p = k_{\mathrm{gb}}\gamma_{\mathrm{gb}}$ where k_{gb} and γ_{gb} are the grain boundary curvature and energy per unit area. Then, grain boundary velocity has the form:

$$v_{\mathrm{gb}} = K_{\mathrm{gb}}\,k_{\mathrm{gb}} \tag{16}$$

where $K_{\mathrm{gb}} = M_{\mathrm{gb}}\gamma_{\mathrm{gb}}$ and we call it the grain boundary constant.

In Equation 16, it is implicit that grain boundary velocity is proportional to the inverse of the boundary curvature radius and that the mobility has a constant value. As it is known, for several cases mobility changes during grain growth and scaling may not hold [24]. Hence, this approximation is not valid for such cases. In addition, we have that the mobility of inclusion particles and/or pores may be proportional to r_{gbc}^{-2}, r_{gbc}^{-3}, or r_{gbc}^{-4}, depending on the assumed mechanism and particle shape [15]. r_{gbc} is the grain boundary curvature radius. In our model, particle shape is a constant since we only take into account normal grain growth. Considering any of this kind of dependences for the grain boundary velocity does not change the qualitative results.

Surface migration is controlled by surface diffusion. Then we have [11]

$$\dot{u}_{\mathrm{s}} = -\frac{2\gamma_{\mathrm{ps}}\Omega\delta D_{\mathrm{s}}}{k_{\mathrm{B}}T}\nabla^2 k_{\mathrm{ps}} \tag{17}$$

where the classical $k_{\mathrm{B}}T$ is Boltzmann's constant times the absolute temperature, Ω represents the atomic volume, δD_{s} is the surface-boundary width times its diffusion coefficient, $\dot{u}_{\mathrm{s}}$ is the normal displacement rate of the pore surface, γ_{ps} is the specific surface energy, and k_{ps} is the pore surface curvature.

Pore surface curvature for the mesocell (Fig. 1) may be written as $k_{\mathrm{ps}} = 1/r$. Taking into account Equations 7 and 17, pore decrease velocity has the form:

$$v_{\mathrm{pd}} = \frac{4\gamma_{\mathrm{ps}}\Omega\delta D_{\mathrm{s}}}{k_{\mathrm{B}}T}k_{\mathrm{ps}}^3 = K_{\mathrm{ps}}k_{\mathrm{ps}}^3 \tag{18}$$

being K_{ps} the pore surface constant.

The scaling principle for the mesocell (Fig. 1) may be written in the following form:

$$\lambda(1) = n\lambda(n) \tag{19}$$

where λ represents the cell dimensions. Finally, we may state that:

$$\begin{aligned}v_{\mathrm{gb}}(n) &= n\,v_{\mathrm{gb}}(1)\\ v_{\mathrm{pd}}(n) &= n^3 v_{\mathrm{pd}}(1)\end{aligned} \tag{20}$$

By combining Equations 14, 16, 18 and 20, the system evolution rate and pore decrease velocities can be obtained from the following equations

$$\begin{aligned}v_{\mathrm{se}} &= K_{\mathrm{gb}}n^2\frac{l_{\mathrm{s}}}{l}F_{\mathrm{M}}\\ v_{\mathrm{pd}} &= K_{\mathrm{ps}}k_{0\mathrm{P}}^3 n^3\\ v_{\mathrm{pd}}^{\mathrm{I}} &= K_{\mathrm{ps}}k_{0\mathrm{P}}^{\mathrm{I}^3} n^3\end{aligned} \tag{21}$$

where F_{M} is a geometrical factor related to the curvature of the grain contacts and may take the values $8/\sqrt{2}$ $k_{0\mathrm{C}_{12}}$, $2k_{0\mathrm{C}_1}$, and $2k_{0\mathrm{C}_2}$.

2.3. Curvature evolution

The assumption that pores are cylinders and grain boundaries are planes is an approximation to calculate the viscous properties and density. In order to have a closed mathematical problem, it is necessary to obtain the dependences of the pore decrease velocities and system evolution rate on sintering time. As is widely known, starting from the interface curvature, the driving pressure must be calculated and we may obtain the mesostructural evolution. In the present work, as was already pointed out, scaling is imposed to the topology of the mesocell. Hence, the way the mesostructure evolutes is imposed. Setting the initial values to interface curvatures imply that the dihedral angles are set as well.

Therefore, we only set the initial grain boundaries curvatures $k_{0C_{12}}$, k_{0C_1}, and k_{0C_2}; and initial pore curvatures $k_{0\mathrm{p}}$ and $k^{\mathrm{I}}_{0\mathrm{p}}$. As scaling holds, increasing the scale of the structure by n reduces all curvatures by $1/n$ [19]. For our problem, we set $F_{\mathrm{M}} = 8/\sqrt{2}\, k_{0C_{12}} = 2k_{0C_1} = 2k_{0C_2}$ and $k^{\mathrm{I}}_{0\mathrm{p}} = \beta^{1/3} k_{0\mathrm{p}}$, being β a constant factor. Then, we have:

$$v^{\mathrm{I}}_{\mathrm{pd}} = K_{\mathrm{ps}} k^{\mathrm{I}^3}_{0\mathrm{p}} n^3 = K_{\mathrm{ps}} \left(\beta^{1/3} k_{0\mathrm{p}}\right)^3 n = \beta v_{\mathrm{pd}} \tag{22}$$

Taking into account the $r(t)$ dependence of Equations 8 and 22, we may say:

$$\begin{aligned} 0 &= \alpha^{\mathrm{I}}_0 - \frac{\beta}{l_{\mathrm{s}}} \int_0^{t_9} v_{\mathrm{pd}}(t')\, \mathrm{d}t' \\ \alpha_9 &= \alpha_0 - \frac{1}{l_{\mathrm{s}}} \int_0^{t_9} v_{\mathrm{pd}}(t')\, \mathrm{d}t' \end{aligned} \tag{23}$$

where t_9 is the time of the $n^{\mathrm{I}}_{\mathrm{p}}$ pore collapse ($\rho_{\mathrm{pc}} = 0.9$).

From Equation 23, we can obtain that:

$$0 = \alpha^{\mathrm{I}}_0 - \beta(\alpha_0 - \alpha_9) \tag{24}$$

Up to this point the statement of the mathematical formulation is completed. The equation system formed by Equations 4, 5, 8 and 21 can be solved numerically (Appendix 2). Then, the pore decrease and the system evolution rate are obtained. First, it is necessary to find α_0 and α^{I}_0 and they are obtained solving the equation system formed by Equations 10 and 24, setting the value of β. Starting from the pore decrease velocity, v_{pd}, and the system evolution rate v_{se}, all the variables of interest may be obtained. Commonly, sintering models report the viscous coefficients and the sintering stress. They are also calculated.

2.4. Viscous coefficients

Viscosity may be obtained by calculation of the force through the contacts. Following the methodology proposed by Riedel *et al*. [8], we have:

$$\nabla^2 \sigma_{\mathrm{n}} = -\frac{k_{\mathrm{B}} T}{\Omega \delta D_{\mathrm{b}}} u_{\mathrm{n}} = -\frac{\gamma_{\mathrm{gb}}}{K_{\mathrm{gb}} \delta^2 s} \dot{u}_{\mathrm{n}} \tag{25}$$

This equation is solved with the boundary condition

$$\sigma_{\mathrm{n}} = 2\gamma_{\mathrm{ps}} k \tag{26}$$

where σ_{n} is the normal stress on the boundary, δD_{b} is the grain-boundary width times its diffusion coefficient, $\dot{u}_{\mathrm{n}}$ is the normal displacement rate of the boundary, and k is the grain curvature at the junction grain-grain-pore. In Equation 25, we consider that the diffusion coefficient and the mobility are related by the relation:

$$M_{\mathrm{gb}} = \left(\frac{D_{\mathrm{b}}}{k_{\mathrm{B}} T}\right)\left(\frac{\Omega}{s\delta}\right) \tag{27}$$

where $s = h d_{\mathrm{C}}$ is the contact area between grains. This relation considers the atomic-jump mechanism across the border. For other mechanism other relations may be found, but in principle mobility and diffusion are related by the Nernst-Einstein equation [15].

Finally, the normal stress, σ_{n}, can be calculated. Integrating it over the contact surface and adding the surface tension along its perimeter, $2\gamma_{\mathrm{ps}} h$, the normal force, F_{n}, exerted on the boundary is

$$F_{\mathrm{n}} = 2\gamma_{\mathrm{s}}(h + ks) + \frac{1}{12} \frac{\gamma_{\mathrm{gb}}}{K_{\mathrm{gb}} \delta^2} \dot{u}_{\mathrm{n}} d^2_{\mathrm{C}} \tag{28}$$

where d_{C} is represented in Fig. 1 and reported in Table I.

So, the energy rate equality can be written in the following form:

$$\dot{W} = \sum_p \dot{u}^{(\mathrm{p})}_{\mathrm{n}} F^{(\mathrm{p})}_{\mathrm{n}} = V \sigma_{\mathrm{ij}} \dot{\varepsilon}_{\mathrm{ij}} \tag{29}$$

where σ_{ij}, $\dot{\varepsilon}_{\mathrm{ij}}$ are the stress tensor and the deformation rate tensor, respectively. The index p runs along all the contact grains in the mesocell.

Considering $\sigma_{\mathrm{ij}} = C_{\mathrm{ijkm}} \dot{\varepsilon}_{\mathrm{km}} + \delta_{\mathrm{ij}} \sigma_{\mathrm{s}}$, where σ_{s} is the sintering stress, the viscous coefficients can be expressed as

$$C_{\mathrm{ijkm}} = \frac{1}{V} \sum_p \frac{\gamma_{\mathrm{gb}} d^2_{\mathrm{C(p)}}}{12 K_{\mathrm{gb}} \delta^2} n^{(\mathrm{p})}_{\mathrm{i}} n^{(\mathrm{p})}_{\mathrm{k}} q^{(\mathrm{p})}_{\mathrm{j}} q^{(\mathrm{p})}_{\mathrm{m}} \tag{30}$$

where $n^{(\mathrm{p})}_{\mathrm{i}} = q^{(\mathrm{p})}_{\mathrm{j}} / q^{(\mathrm{p})}$, $q^{(\mathrm{p})}_{\mathrm{j}}$ are the normal to the contact surface and the contact radii vector, respectively. Table I

TABLE I Contact radii vector, $\bar{q}(q_1, q_2)$, module of contact radii, ($q = \sqrt{q_1^2 + q_2^2}$), normal to the contact surface, $\bar{n}(n_1, n_2)$, and contact area, $hd(C_{\mathrm{i}})$ for the contacts C_1, C_2, and C_{12} shown in Fig. 1. The superscript p runs along all the contact grains in the mesocell

Contacts	Contact vector radii $(q^{(\mathrm{p})}_1, q^{(\mathrm{p})}_2)$	Module of contact radii q	Normal to the contact surface $(n^{(\mathrm{p})}_1, n^{(\mathrm{p})}_2)$	Contact area $hd(C_1)$
C_1	$(l/4n, 0)$	$l/4n$	$(1, 0)$	$h(l/4n - 2r_{\mathrm{n}})$
C_2	$(0, l/4n)$	$l/4n$	$(1, 0)$	$h(l/4n - 2r_{\mathrm{n}})$
C_{12}	$(l/8n, \pm l/8n)$	$\sqrt{2l}/8n$	$\sqrt{2}(1, \pm 1)$	$h(\sqrt{2l}/8n - r_{\mathrm{n}} - r^{\mathrm{I}}_{\mathrm{n}})$

lists the magnitudes and calculations performed regarding contact radii vector, $\bar{q}(q_1, q_2)$, module of contact radii, ($q = \sqrt{q_1^2 + q_2^2}$), normal to the contact surface, $\bar{n}(n_1, n_2)$, and contact area, $hd(C_i)$.

Hence, the viscous coefficients (see Table I) may be written as:

$$C_{1111} = \frac{1}{h}\frac{\gamma_{gb}}{12K_{gb}\delta^2}\frac{1}{4n^2}\left[\left(\frac{l}{4} - 2r\right)^2 + 12\left(\frac{\sqrt{2}l}{8} - r - r^I\right)^2\right] \quad (31)$$

$$C_{1212} = \frac{1}{h}\frac{\gamma_{gb}}{12K_{gb}\delta^2}\frac{1}{4n^2}\left(\frac{l}{4} - 2r\right)^2 \quad (32)$$

$$G = C_{1212} = C_{1122}$$

$$K = \frac{1}{3}(C_{1111} + C_{1122}) \quad (33)$$

The main transport mechanism giving rise to densification is assumed to be the grain boundary diffusion in the contact area between particles. Surface diffusion at the pore surfaces influences densification because it governs the material transport from the pore surfaces to the neck. A similar picture is considered by Svoboda *et al.* [11]. Viscosity coefficients show its straight dependence on K_{gb} (see Equations 31 and 32). The dependences on K_{ps} and K_{gb} are implicit in the parameters n, l, and r describing the cell transformations.

2.5. Sintering stress

The sintering stress is calculated by the following expression:

$$\sigma_s = -3K\dot{\varepsilon}_\rho \quad (34)$$

3. Results

For the sake of performing computation, we take $l_s = 1$, and parameter h may not be part of codes. Numerical values are required for n_0, k_{0p}, β, and F_M; arbitrarily, with a little intuition, and trial and error, the selected numbers are 20, 0.25, 0.05 and 1. For simplicity we consider $K_{gb} = 1$. Then, for $K_{ps} > K_{gb}$, we have $K_{ps} = 1.2$ and for $K_{ps} < K_{gb}$; $K_{ps} = 0.8$. Therefore, viscosity is reported as $G/(\gamma_{gb}10^5/48\ K_{gb}\delta^2)$ and sintering stress as $\sigma_s/(\gamma_{gb}10^5/48\ K_{gb}\delta^2 ut)$ where ut stands for unit times.

Fig. 2 shows the time dependence for the pore decrease velocity and system evolution rate.

The time dependence of pore radius, mesocell lateral dimensions, and interface area, are plotted in Fig. 3. As expected, all these magnitudes decreased with increasing time. The top axis in Fig. 4 represents the time dependence of the average grain size, while the botton axis shows the average grain size dependence on relative density. Notice that the average grain size increases with increasing time and density. The influence of interface properties on time dependence is negligible, but they do affect the density dependence.

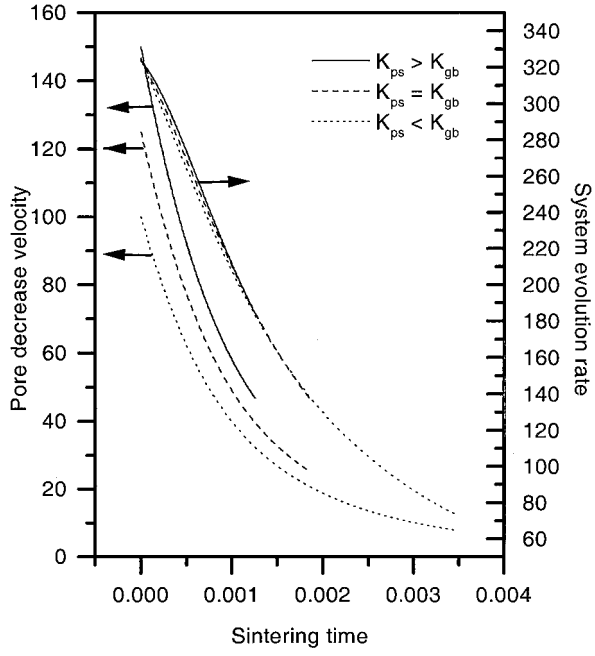

Figure 2 Dependence of the pore decrease velocity, v_{pd}, and system evolution rate, v_{se}, on time. Both parameters decrease with time. Pore decrease velocity is influenced by interface properties while system evolution rate is not affected.

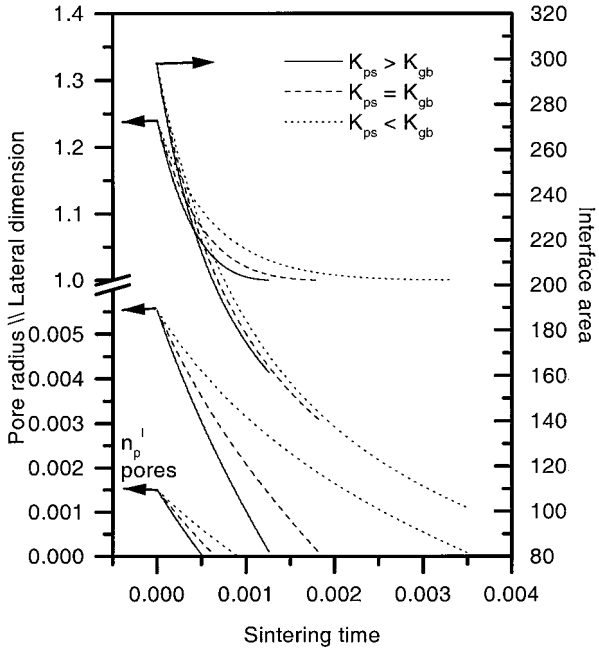

Figure 3 Dependence of the pore radius, r and r^I, cell lateral dimension, l, and interface area, A_{int}, on time. All the mentioned magnitudes decrease with time and are affected in the same way by the interface properties. The decrease of the grain boundary constant accelerate the decrease of the shown dependences.

The time dependences of the relative density and densification rate are shown in Fig. 5. Notice that relative density increases with increasing time, and density increases more rapidly when $K_{ps} > K_{gb}$. As to the dependence of the densification rate, the highest values occur when $K_{ps} > K_{gb}$, during the first time units. However, as densification proceeds, the situation is inverted. The dependence of the densification rate on relative density is presented in Fig. 6. Notice that, for all the relative density values, the highest values for the

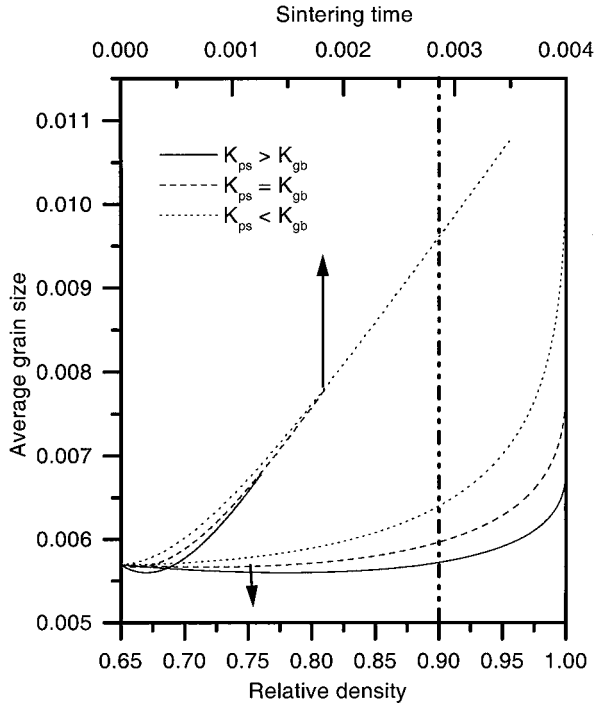

Figure 4 Dependence of the average grain size on time (bottom axis) and relative density (top axis). Average grain size increases as sintering occurs. Interface properties influence the dependence on relative density and does not on time.

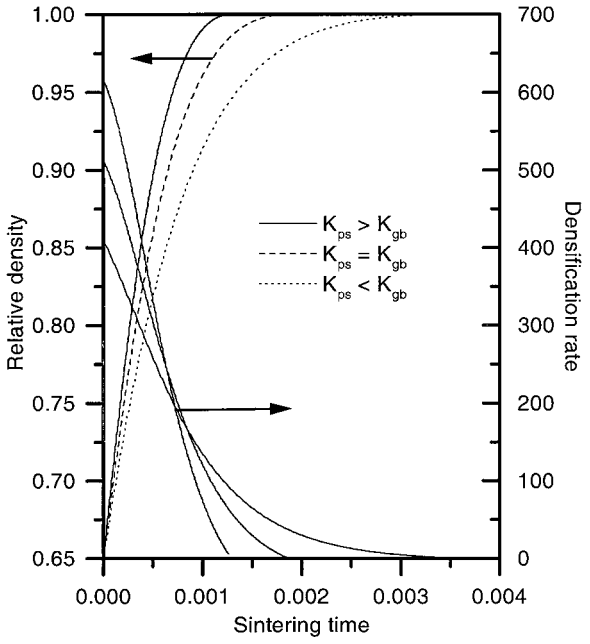

Figure 5 Dependence of relative density, ρ, and densification rate, $\dot{\varepsilon}_\rho$, on time. Relative density increase with time and densification rate decrease. Interface properties affect both dependences.

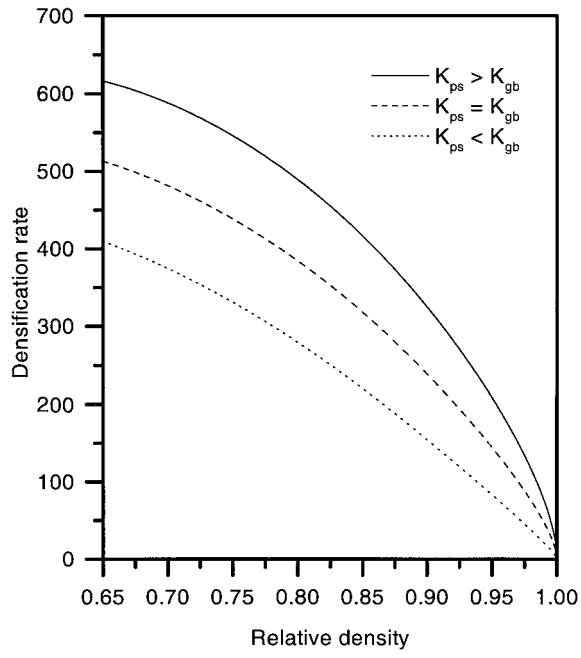

Figure 6 Dependence of the densification rate, $\dot{\varepsilon}_\rho$, on the relative density. Densification rate decreases as relative density increases. The decrease of the grain boundary constant favors the densification rate.

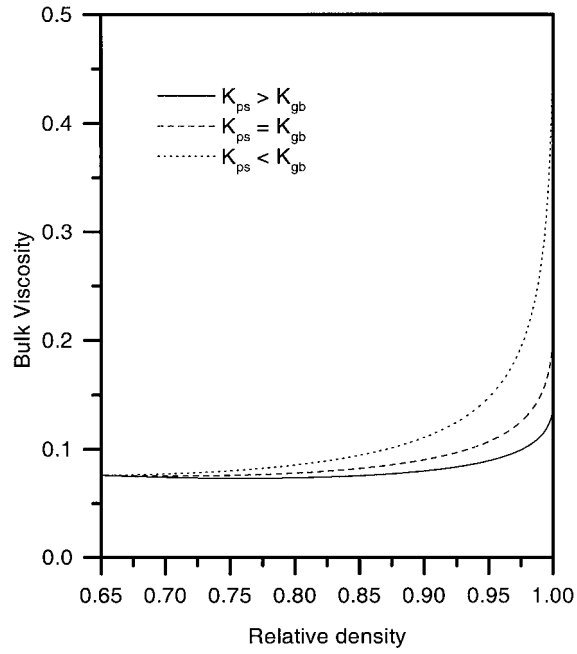

Figure 7 Dependence of the bulk viscosity, K, on the relative density. The bulk viscosity increase with the relative density. The decrease of the grain boundary constant provokes the bulk viscosity to decrease favoring densification.

densification rate occur for $K_{ps} > K_{gb}$, and the lowest for $K_{ps} < K_{gb}$.

Figs 7, 8 and 9 show the typical macroscopic magnitudes reported in sintering models: bulk and shear viscosities, and sintering stress.

4. Discussion

It is widely known from theoretical and experimental studies that the sintering process is faster during the initial time units. As shown in Fig. 2, this tendency is evident for the calculated decreases in pore decrease velocity and system evolution rate. Note that the interface properties have a negligible effect on the evolution rate. On the other hand, the pore decrease velocity is significantly influenced by the interface constants. The higher the pore surface constant, the higher the velocities obtained from calculations.

As expected, there was a tendency of the pore radius and cell lateral dimension to decrease with increasing time (Fig. 3). Otherwise, densification would not be

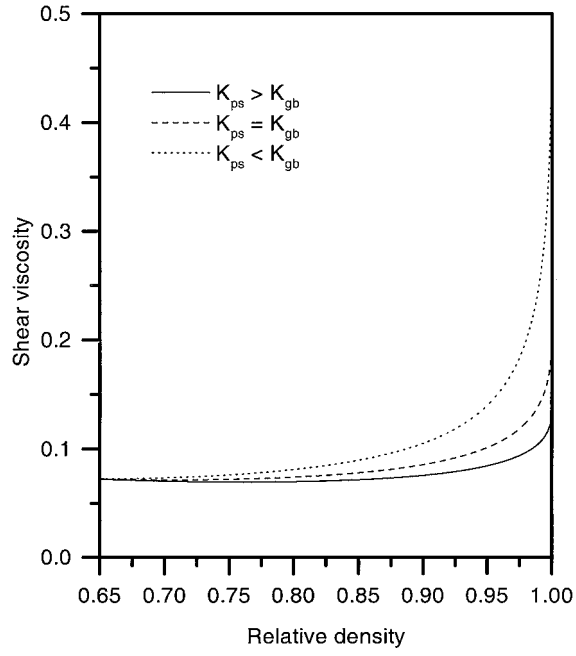

Figure 8 Dependence of the shear viscosity, G, on the relative density. The dependence on interface properties behaves almost as equal as the one for the bulk viscosity.

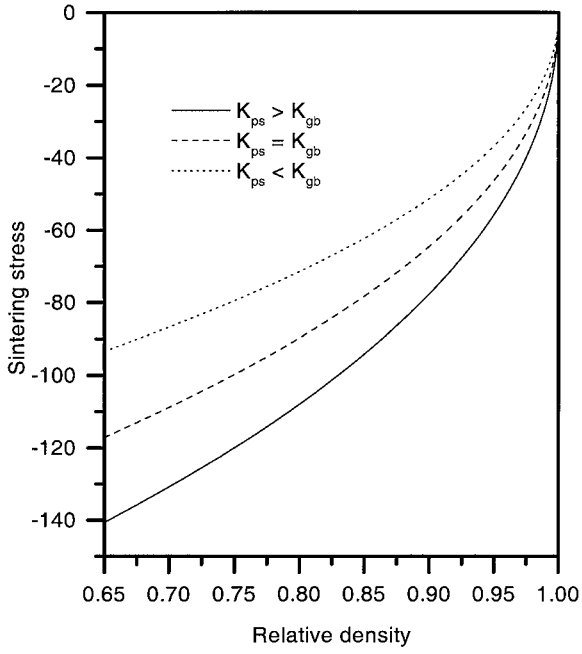

Figure 9 Dependence of the sintering stress, σ_s, on the relative density. The general tendency of the sintering stress is to decrease its absolute value. This tendency is intensified for $\rho = 0.9$–1.0.

achieved. Fig. 3 also illustrates the reduction of the interface area. This result agrees completely with the generally accepted idea that the driving force for sintering is the decrease in the surface free energy. It is known that energy and interface area are linearly related by the free energy per unit area of the grain boundary and the pore surface.

The relation $G^m - G_0^m = K_{gg}t$, where G, G_0 and K_{gg} are, respectively, grain size, initial grain size, and a given constant, is well known in scientific literature. The kinetic grain growth exponent, m, depends on the grain growth mechanisms. As result of scaling, normal grain growth takes place and m is expected to be equal 2 [19]. The fitting between the mentioned relation and the dependence of Fig. 4 gives the best results for $K_{gg} = 2.8$, but this fitting is not good enough. We believe that this litter difference is due to that in the present model grain growth is taking place together with pore decrease and this last fact with the implicit approximation of Equation 12 influence the time dependence of the average grain size. Fig. 4 shows that the interface properties do not affect the dependence of the average grain size on sintering time. This is because, the sintering mechanism is the same for all the cases considered. On the other hand, the dependence of grain size on relative density is affected by the interface constants. This is because of the influence of the interface properties on the relative density time dependence, as shown in Fig. 5.

The dependence of average grain size on density is also known as *microstructure development map*. Note in Fig. 4 that, as density increases, so do grain growth, and grain growth rate. According to experimental data [25, 26], there is virtually no grain growth when the relative density is below 0.9 (stage I). Approximately 90% of grain growth occurs above this value (stage II). The tendency shown in Fig. 4 is qualitatively consistent with this behavior. It is known [27] that there is a competition between densification and grain growth. During the first sintering time units, for low density materials, the free energy of the system decreases by densification, rather than by grain growth. As density increases, the situation reverses itself. It is worthily to point out that, in the present model, the occurrence of grain growth (related to system evolution) and pore decrease does not start form energy minimization, but the physical picture is congruent with the mentioned energy statement.

The density and the densification rate dependences reported in Fig. 5 are similar to the experimental results reported by Durruthy *et al.* [28] for Nb-dopped PZT ceramics. These authors have shown experimentally that Niobium doping inhibits grain growth and enhances densification. Fig. 10 illustrates the Durruthy results. From Figs 5 and 10, it may be concluded that doping favors the pore interface constant K_{ps} over that of the grain boundary interface K_{gb}.

Fig. 5 also describes the findings of Han *et al.* [29] for Al-doped ZnO ceramics at temperatures above 1200°C, and at sintering times longer than some critical values, which depend on the Al-doping level.

The comparison between the results of this model and those of Han *et al.* is not straightforward. They reported that, for sintering times of less than 150-min at 1200°C, the fired densities of Al-doped ZnO samples were lower than those of pure ZnO. These results seem to contradict this model and the above interpretation of Durruthy's results. Hang *et al.* suggested that there was a competition between grain growth and sintering potential in the materials they studied. They concluded that the densification rate decreases because of the reduction in the sintering potential, due to the *drag* caused by *pinning*. As long as pinning is effective, scaling is being violated. This effect resulted from the presence of a second phase ($ZnAl_2O_4$). The grain boundary pinning

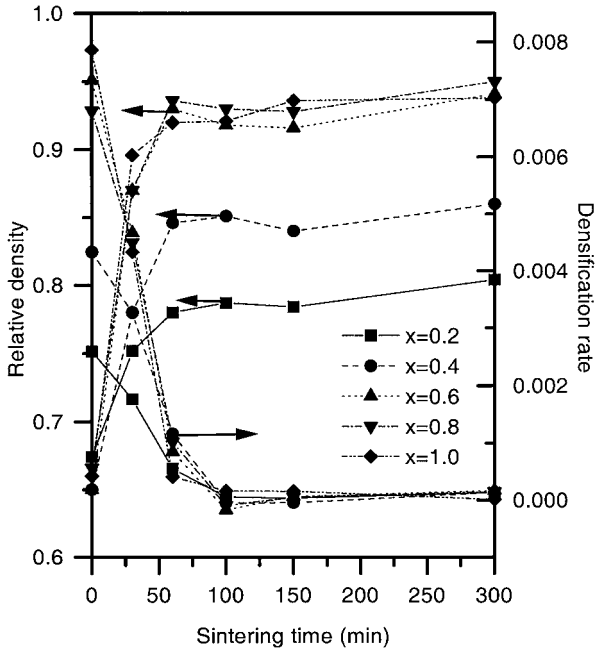

Figure 10 Dependence of the relative density, ρ, and densification rate, $\dot{\varepsilon}_\rho$, on the sintering time for PZT + x% wt Nb_2O_5 powder compact, where $x = 0.2$ (■), 0.4 (●), 0.6 (▲), 0.8 (▼), 1.0 (♦), sintered at 1250°C, indicating that the highest densities are reached for the highest Nb concentrations. Effective grain boundary mobility may be written as $M_{ef} = M_{gb}/(1 + Ax)$, where A is a constant.

can be clearly observed in the SEM micrograph in their paper. In the present model, grain boundary pinning is not taken into account. Equation 15 is assumed to be valid at all times. According to the atomistic simulation performed by Upmanyu *et al*. [22], pinning of grain boundaries by vacancies causes a deviation from the steady-state grain boundary migration. This means that the linearity between the driving force and the interface velocity, implicit in Equation 15, is not valid during pinning. Fig. 9 shows that the interface properties does not change essentially the sintering stress behavior. This fact is consistent with the assumption of Hang *et al*. that the force exerted by the dragging particles results in a decrease in the sintering potential. After 150-min of sintering and at higher temperatures, grain growth is considered to be the dominant mechanism for Al-doped ZnO ceramic sintering. For this interval, it may be concluded that doping favors the pore interface constant over that of the grain boundary interface. In the above interval, the model predictions agree with experimental results.

Castro *et al*. [30] studied the Nb-doped PZT ceramics. Although, they performed careful SEM observations, they found no pinning in their materials. We think that the absence of the pinning effect explains the coincidence, between the predictions of the present model and the results of Durruthy *et al*. [28], for all the values of the sintering time.

Cahn's model, outlined by Rahaman [31], postulates that the total drag force on the boundary is the sum of the intrinsic drag and the drag due to dopant atoms. This may be interpreted as a decrease of the effective mobility. In fact, in Cahn's model there is a relation that supports this conclusion, under certain considerations. Dopant atoms are expected to reduce the grain boundary mobility. This drag effect induces grain growth inhibition, for instance, the effect shown in Fig. 4 as K_{gb} decreases. The interface energy must increase as result of dopant atoms at grain boundaries. However, the drag effect caused by impurities is dominant. Based on the previous assumption that doping favors K_{ps} over K_{gb}, we conclude that grain growth inhibition favors densification (Figs 4 and 5). This is exactly the effect of doping PZT ceramics with Nb experimentally observed by Durruthy *et al*. [28].

From Fig. 6, it may be concluded that the higher the pore surface constant, or the lower the grain boundary constant, the higher the densification rate. This statement is also valid for the behaviors illustrated in Fig. 5. The interceptions of the densification rate curves on time is a consequence of the fact that, after the system with higher densification has reached the highest densities, the densification rate exhibits a very strong tendency to decrease. This tendency appears "later" in the other lower density systems of this model, because of lower densification rates.

In Figs 7 and 8, it can be observed that, as the grain boundary constant decreases, the bulk and shear viscosity do as well. This behavior may be interpreted as if densification or sintering were favored. Also, it can be observed that viscosities increase with density. This supports the already mentioned fact that sintering is faster during the initial time units.

In Fig. 9, it can be noticed that the absolute value of sintering stress decreases as density increases. In addition, it may be seen that approximately half of the sintering stress decrease occurs during the stage II ($\rho = 0.9$–1.0) and this does not correspond to half of the density increase. This behavior is related with the competition between the pore decrease size, favoring the increase of the absolute value of sintering potential, and the grain growth, which disfavors the mentioned magnitude [31]. Comparing the average grain size density dependence (Fig. 4) with the one of Fig. 9, it can be noticed that the most significant drop for the absolute value of the sintering stress occurs when most of the grain growth takes place.

The model presented herein has some simplifications and assumptions, so it does not consider effects like pinning, some kinetic aspects of pore movement, and a more realistic picture of grain growth phenomena and coarsening. This model can also be improved by incorporating the different sintering mechanisms, and by considering a more realistic energetic picture. A finer study is out of the scope of the present work. Nevertheless, a modest insight has been gained.

5. Conclusions

A model considering densification and grain growth as a result of a proposed geometry with scaling imposed has been stated. With this model, it is possible to study the effects of the interface properties on densification. It can be concluded that a decrease in the interface constant for the grain boundary, or an increase in the pore surface constant, will increase the densification rate,

as long as the steady-state grain boundary migration is valid. This model confirms that grain growth inhibition, obtained by reducing the grain boundary mobility, is a means to increase densification. This result is consistent with some previous experimental results reported in scientific literature.

As in most sintering models, the viscosities and the sintering potential are reported. It should be noted that, as the interface constants for the grain boundary are disfavored over the pore surface ones, viscosities tend to decrease. This means, again, that densification is promoted. It must be noticed that interface properties do not affect the qualitative behavior of the sintering potential.

Acknowledgement

This study was sponsored by CONACYT, research project 31234-U.

We are also indebted to Professor Rajendra K. Bordia (Materials Science and Engineering, University of Washington), for his advise and stimulating discussions on this project.

Appendix 1: Interface velocities

According to Fig. 11, for contacts C_1 and C_2, it is possible to state that between two subsequent values of n, we have:

$$d_u = d_u^n - d_u^{n+1} \tag{A1.1}$$

where

$$\begin{aligned} d_u^k &= \frac{l}{2n} \\ d_u^{k+1} &= \frac{l}{2(n+1)} \end{aligned} \tag{A1.2}$$

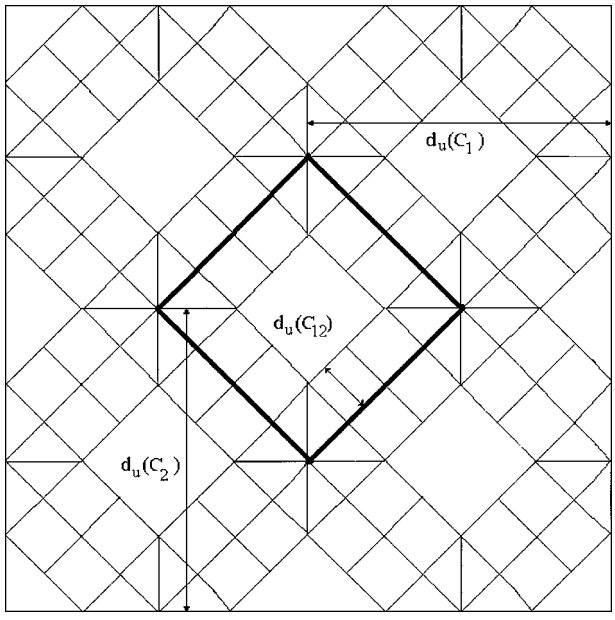

Figure 11 The $l \times l$ plane view of the mesocell for $n = 2$. The parameters $d_u(C_1)$, $d_u(C_2)$, and $d_u(C_{12})$ represent the grain boundary displacement for the grain boundary C_1, C_2, and C_{12} between $n = 1$ and $n = 2$. The double line represents some of the C_{12} grain boundary for $n = 1$.

then

$$d_u = \frac{l}{2n(n+1)} \tag{A1.3}$$

From Equation 8, we may rewrite:

$$n_2 = n_1\left(1 - \frac{1}{l_s}\int_{t_1}^{t_2} v_{se}(t')\,dt'\right) \approx n_1\left(1 - v_{se}(\bar{t})\frac{\Delta t}{l_s}\right) \tag{A1.4}$$

where n_1 and n_2 correspond to t_1 and t_2, and $\bar{t} \approx (t_1 + t_2)/2$.

Let us suppose that $n_1 = n + 1$ and $n_2 = n$, then

$$n = (n+1)\left(1 - v_{se}\frac{\Delta t}{l_s}\right) \tag{A1.5}$$

As follow, the interface velocity is written in the following way:

$$\frac{du_1}{dt} \approx \frac{d_u}{\Delta t} = \frac{l}{l_s}\frac{1}{2n}v_{se} \tag{A1.6}$$

Analogously, du_{12}/dt is obtained.

Appendix 2: Computation of system evolution rate and pore decrease velocities

Solving the equation system formed by Equations 4, 5, 8 and 21 the pore decrease and the system evolution velocities can be calculated, but the integral in Equation 8 implies some numerical difficulties when we are solving the equation system.

We propose the following method to solve this problem:

Equation 8 may be written as:

$$\begin{aligned} n(t) &\approx n_0\left(1 - \frac{1}{l_s}\sum_{i=1}^{N} v_{se}(\bar{t})\Delta t\right), \\ r(t) &\approx r_0 - \sum_{i=1}^{N} v_{pd}(\bar{t})\,\Delta t \end{aligned} \tag{A2.1}$$

for the present calculations Δt is taken very small in order to minimizes the error, unlike (A1.5).

First, we solve the system for $t = 0$, the equations take the following form

$$\begin{aligned} l^2(0) &= l_s^2 + 14\pi\alpha_0^2 + 16\pi\alpha_0^{I^2} \\ n(0) &= n_0 \\ r(0) &= r_0 \\ r^I(0) &= r_0^I \\ r_0 &= \alpha_0 l_s \\ r_0^I &= \alpha_0^I l_s \\ v_{se}(0) &= K_{gb}n^2(0)\frac{l_s}{l(0)}F_M \\ v_{pd}(0) &= K_{ps}k_{0p}^3 n^3(0) \end{aligned} \tag{A2.2}$$

The cell lateral dimension, l, decreases with time, then

$$\Delta l^2 = 14\pi\left(r_1^2 - r_2^2\right) + 16\pi\left(r_1^{I^2} - r_2^{I^2}\right) \tag{A2.3}$$

Taking into account that Equation 8 may be written as

$$r_2 = r_1 - \int_{t_1}^{t_2} v_{pd}(t')\,dt' \approx r_1 - v_{pd}(\bar{t})\,\Delta t, \quad \text{(A2.4)}$$

and Equation A2.3, the parameter, l, may be written as

$$\begin{aligned} l^2(t) = l^2(t-\Delta t) - 14\pi((2r(t-\Delta t) \\ - v_{pd}(t)t)v_{pd}(t)t) - 16\pi((2r(t-\Delta t) \\ -\beta v_{pd}(t)t)\beta v_{pd}(t)t) \end{aligned} \quad \text{(A2.6)}$$

Finally, the system evolution and pore decrease velocities are calculated consecutively solving the equation systems formed by Equation A2.6 and the following equations

$$\begin{aligned} n(t) &= n(t-\Delta t) - n_0 v_{se}(t)\frac{\Delta t}{l_s} \\ v_{se}(t) &= K_{gb} n^2(t)\frac{l_s}{l(t)} F_M \\ v_{pd}(t) &= K_{ps} k_{0p}^3 n^3(t) \end{aligned} \quad \text{(A2.7)}$$

References

1. J. FRENKEL, *J. Phys. USSR* **9** (1945) 385.
2. J.K. MACKENZIE and R. SHUTTLEWORTH, *Proc. Phys. Soc. Lond.* **62** (1949) 833.
3. R. K. BORDIA and G. W. SCHERER, *Acta Metall.* **36** (1988) 2393.
4. G. W. SCHERER, *J. Amer. Ceram. Soc.* **74** (1991) 1523.
5. J. I. MARTÍNEZ-HERRERA and J. J. DERBY, *ibid.* **78** (1995) 645.
6. G. A. L. VAN DE VORST, R. M. M. MATHEU and H. K. KUIKEN, *J. Comput. Phys.* **100** (1992) 50.
7. R. L. COBLE, *J. Appl. Phys.* **32** (1961) 787.
8. H. RIEDEL, H. ZIPSE and J. SVOBODA, *Acta Metall. Mater.* **42** (1994) 445.
9. H. RIEDEL, V. KOZAK and J. SVOBODA, *ibid.* **42** (1994) 3039.
10. J. SVOBODA, H. RIEDEL and H. ZIPSE, *ibid.* **42** (1994) 435.
11. J. SVOBODA and H. RIEDEL, *ibid.* **43** (1995) 499.
12. J. PAN and A. C. F. COCKS, *ibid.* **43** (1995) 1395.
13. N. D. APARICIO and A. C. F. COCKS, *ibid.* **43** (1995) 3873.
14. W. ZHANG, J. H. SCHNEIBEL and C.-H. HSUEH, *Philos. Mag.* A **70** (1994) 1107.
15. W. D. KINGERY, H. K. BOWEN and D. R. UHLMANN, "Introduction to Ceramics" (John Wiley & Sons, 1975).
16. A. JAGOTA and G. W. SCHERER, *J. Amer. Ceram. Soc.* **78** (1995) 521.
17. *Idem.*, *ibid.* **76** (1993) 3123.
18. A. JAGOTA, K. R. MIKESKA and R. K. BORDIA, *ibid.* **73** (1990) 2266.
19. W. W. MULLINS, *Acta Mater.* **17** (1998) 6219.
20. *Idem.*, *ibid.* **11** (1989) 2979.
21. *Idem.*, *J. Appl. Phys.* **59** (1986) 1341.
22. M. UPMANYU, R. W. SMITH and D. J. SROLOVITZ, *Inter. Sci.* **6** (1999) 41.
23. M. UPMANYU, D. J. SROLOVITZ, L. S. SHVINDLERMAN and G. GOTTSTEIN, *Acta Mater.* **47** (1999) 3901.
24. M. FURTKAMP, G. GOTTSTEIN and L. S. SHVINDLERMAN, *Inter. Sci.* **6** (1998) 277.
25. J. KANTERS, U. EISELE and J. RÖDEL, *J. Amer. Ceram. Soc.* **84** (2001) 2757.
26. P. DURAN, *Bol. Soc. Esp Cerám. Vidrio* **38**(5) (1999) 403.
27. J. M. TING and R. Y. LIN, *J. Mater. Sci.* **29** (1994) 1867.
28. M. D. DURRUTHY, L. FUENTES, M. HERNANDEZ and H. CAMACHO, *J. Mater. Sci.* **9** (2000) 2311.
29. J. HAN, P. Q. MANTAS and A. M. R. SENOS, *J. Mater. Res.* **2** (2001) 459.
30. J. CASTRO, T. DE LOS RÍOS and L. FUENTES, *Mater. Manufac. Proc.* **2** (2000) 301.
31. M. N. RAHAMAN, "Ceramic Processing and Sintering" (Marcel Dekker, Inc., 1995).

Received 10 September 2002
and accepted 20 May 2003